Creaseness Measures for CT and MR Image Registration

Antonio M. López, David Lloret, Joan Serrat
Computer Vision Center and Departament d'Informàtica,
Universitat Autònoma de Barcelona,
Edifici O, 08193–Cerdanyola, Spain.
Tel. +34 3 581 2561, Fax +34 3 581 1670
e–mail : antonio@cvc.uab.es

Abstract

Creases are a type of ridge/valley structures that can be characterized by local conditions. Therefore, creaseness refers to local ridgeness and valleyness. The curvature κ of the level curves and the mean curvature κ_M of the level surfaces are good measures of creaseness for 2–d and 3–d images, respectively. However, the way they are computed gives rise to discontinuities, reducing their usefulness in many applications. We propose a new creaseness measure, based on these curvatures, that avoids the discontinuities. We demonstrate its usefulness in the registration of CT and MR brain volumes, from the same patient, by searching the maximum in the correlation of their creaseness responses (ridgeness from the CT and valleyness from the MR). Due to the high dimensionality of the space of transforms, the search is performed by a hierarchical approach combined with an optimization method at each level of the hierarchy.

1 Introduction

Ridge/valley structures of a grey–level image tend to be at the center of anisotropic shapes. Therefore, they have been used in a number of applications as object descriptors. On the other hand, the mathematical characterization of what is a ridge/valley is far from being a simple issue [5]. Several different mathematical definitions have been proposed which we classify in three groups according to their scope:

- Creases : *local* descriptors that, basically, look for the center of anisotropic shapes.
- Separatrices : *global* descriptors that result of linking the critical points of the image by means of slopelines, dividing it in hill/basin districts. Slopelines are curves which run orthogonal to the level curves, this is, they integrate the image gradient vector field.

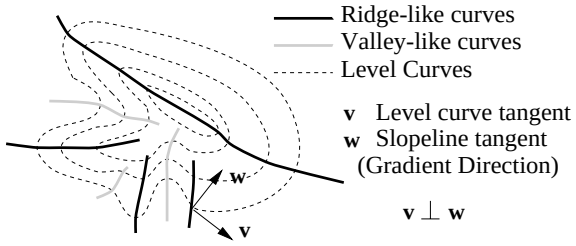

Figure 1: A type of ridge/valley–like curves is defined as the loci of extrema of κ along the $\mathbf{v}$ direction.

- Drainage patterns : channels of water generated by the surface runoff induced in a landscape when it rains. They have a *regional* character.

Yet, in the literature we can find several definitions within the crease class [1]. Among them, the one based on level set extrinsic curvature is particularly useful because of its invariance properties. Given a function $L : \mathbb{R}^d \rightarrow \mathbb{R}$, the level set for a constant g consists of the points $\{\mathbf{x}|L(\mathbf{x}) = g\}$. The variation of g produces all the level sets of L. The simplest situation occurs at $d = 2$, when L can be thought as a topographic relief and the level sets are its level curves. Negative minima of the level curve curvature κ, level by level, form valley–like curves and positive maxima ridge–like curves (Fig. 1) [3]. If we denote as $\mathbf{v}$ the tangent vector to the level curves, these creases are characterized by the following local extremality criterion:

$$e = \nabla\kappa \cdot \mathbf{v} = 0 \qquad (1)$$

where $\nabla e \cdot \mathbf{v} < 0$, $\kappa > 0$ means ridge and $\nabla e \cdot \mathbf{v} > 0$, $\kappa < 0$ valley.

In the 3–d case the straightforward extension of κ for level surfaces is two times the Mean curvature κ_{M} of these surfaces. Since κ_{M} is a non–directional quantity, other authors [7, 12] have applied the extremality

criterion to the principal curvature of the level surfaces which is largest in magnitude.

The direct computation of extremality criteria as (1) involves up to fourth order image derivatives combined into a complex expression (check for example [3] p. 637 for the 2–d case and [7] p. 176 for 3–d). Nevertheless, the extrema of curvature of elongated structures in 2–d and plate–like structures in 3–d are so high that one can circumvent the computational drawback by just computing κ or κ_{M} as creaseness measures and then performing a thresholding. Or just take the creaseness measure itself as a feature, like in the image registration application we present in this paper. This is by no means an infrequent situation but it is precisely for these anisotropic structures that ridge and valley lines are employed.

However, in 2–d for example, the way κ is usually computed gives raise to discontinuities at places where we would not expect any reduction of creaseness because they are at the center of elongated objects and creaseness is a measure of medialness for them. The same problem arises when computing κ_{M} in 3–d.

In Sect. 2 we review the traditional way of computing κ and κ_{M}, analyze the above mentioned problem and propose a first alternative to avoid it. Section 3 we go further and present a second improvement derived in a natural way from the first one and based on the so–called structure tensor. The creaseness measure derived in Sect. 3 is used in Sect. 4 to register CT and MR brain volumes. The results are compared with the *mutual information* algorithm which is considered one of the best for registering images from different sensors. Conclusions are summarized in Sect. 5.

2 Level set extrinsic curvature based on the image gradient vector field

The level set extrinsic curvature in Cartesian coordinates for the two and three–dimensional cases are:

$$\kappa = (2L_xL_yL_{xy} - L_y^2L_{xx} - L_x^2L_{yy})(L_x^2 + L_y^2)^{-\frac{3}{2}} \quad (2)$$

$$\begin{aligned}\kappa_{\mathrm{M}} = \frac{1}{2}\Big(&2(L_xL_yL_{xy} + L_xL_zL_{xz} + L_yL_zL_{yz}) \\ &-L_x^2(L_{yy} + L_{zz}) - L_y^2(L_{xx} + L_{zz}) \\ &-L_z^2(L_{xx} + L_{yy})\Big)(L_x^2 + L_y^2 + L_z^2)^{-\frac{3}{2}} \end{aligned} \quad (3)$$

where L_α denotes the first order partial derivative of L with respect to α, $L_{\alpha\beta}$ the second order partial derivative with respect to α and β. To obtain derivatives of a discrete image L in a well–posed manner we have approximate them by finite differences of the Gaussian–smoothed image:

$$L_\alpha(\mathbf{x};\sigma_{\mathrm{D}}) = \frac{\partial}{\partial\alpha}(L(\mathbf{x}) * G(\mathbf{x};\sigma_{\mathrm{D}})) \approx \delta_\alpha L(\mathbf{x};\sigma_{\mathrm{D}}) \quad (4)$$

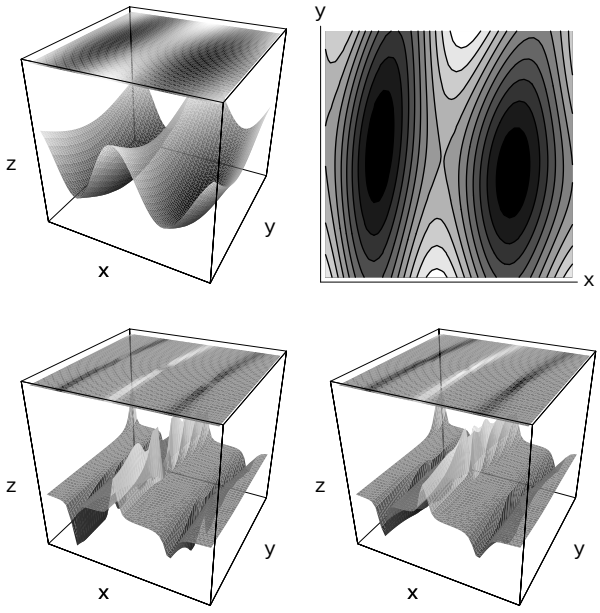

Figure 2: From top to bottom and left to right: (a) relief with regions having valley–like and ridge–like shape, (b) its level curves, (c) κ (notice the gaps), (d) $\bar{\kappa}$.

where δ_α stands for a partial finite difference along the discrete α axis and σ_{D} is the standard deviation of the Gaussian kernel. We use centered finite differences because of their invariance under rigid movements in the image plane and their high approximation order.

In the 2—d case, if we travel along the center of anisotropic structures, we go up and down on the relief, passing through isolated maxima, saddles and minima. We have found that computation of κ according to Eq. (2) produces discontinuities in the creaseness measure around this type of critical points (e.g. Fig. 2), as well as on the center of elongated grey–level objects having a short dynamic range along this center. We have checked that they are produced independently of the scheme we use to approximate derivatives. Moreover, the problem is not due to a low gradient magnitude, since they appear even when the image gradient magnitude is far away from the zero of the machine, this is, Eq. (2) is well–defined. The 3–d measure κ_{M} has analogous problems if it is computed according to Eq. (3). Other 3–d creaseness measures like $L_{\mathbf{pp}}$ (ridgeness) and $L_{\mathbf{qq}}$ (valleyness) [2, 6] – the second order directional derivatives along the principal directions ($\mathbf{p}$ and $\mathbf{q}$) of the level surfaces – also present discontinuities (see [2] p. 386 and [6] p. 83).

To avoid this problem we present an alternative way of computing creaseness based on the level set extrin-

sic curvature. In vector calculus there is a well–known operator called divergence [10] which measures the degree of parallelism of a vector field and, therefore, of its integral lines. The divergence of a d dimensional vector field $\mathbf{u} : \mathbb{R}^d \rightarrow \mathbb{R}^d, \mathbf{u}(\mathbf{x}) = (u^1(\mathbf{x}), ..., u^d(\mathbf{x}))^{\mathrm{t}}$ is defined as:

$$\mathrm{div}(\mathbf{u}) = \sum_{i=1}^{d} \frac{\partial u^i}{\partial x^i} \quad . \tag{5}$$

Now, if we denote by $\mathbf{0}_d$ the d dimensional zero vector, then we can define $\bar{\mathbf{w}}$, the normalized gradient vector field of $L : \mathbb{R}^d \rightarrow \mathbb{R}$, as:

$$\bar{\mathbf{w}} = \begin{cases} \mathbf{w}/\|\mathbf{w}\| & \text{if} \quad \|\mathbf{w}\| > 0 \\ \mathbf{0}_d & \text{if} \quad \|\mathbf{w}\| = 0 \end{cases} \tag{6}$$

where the x^i are the coordinate axes and $\mathbf{w} = (L_{x^1}, ..., L_{x^d})^{\mathrm{t}}$ is the image gradient vector.

It can be shown that the d dimensional level set curvature can be defined as:

$$\kappa_d = -\mathrm{div}(\bar{\mathbf{w}}) \tag{7}$$

where $\kappa_d > 0$ means ridge and $\kappa_d < 0$ valley.

For $d = 2$, Eq. (2) is equivalent to Eq. (7) in the continuous domain. However, and this is the key point, the same derivatives approximation of Eq. (2) and Eq. (7) gives different results, namely, the discretization of Eq. (7) avoids the discontinuities that Eq. (2) produces on creases. The same applies to Eq. (3) and Eq. (7), since $\kappa_{\mathrm{M}} = \kappa_3/2$. Thus, from now on, we denote by κ and $\bar{\kappa}$ the discrete versions of the level set extrinsic curvature according to Eq. (2) and Eq. (7), respectively. Symbols κ_{M} and $\bar{\kappa}_{\mathrm{M}}$ will be used analogously, and for higher values of d, κ_d and $\bar{\kappa}_d$. Figure 2 compares the behavior of κ and $\bar{\kappa}$. Notice how discontinuities disappear now. Furthermore, it can be shown that if we approximate the derivatives of a d dimensional image with centered finite differences then $|\bar{\kappa}_d| \leq d$, reaching $-d$ at minima and d at maxima.

3 Level set extrinsic curvature based on the image structure tensor field

Once we have established $\bar{\kappa}$ and $\bar{\kappa}_{\mathrm{M}}$ as good creaseness measures, we can go further and improve them by modifying the gradient vector field of the image before applying the divergence operator. Given the usual configurations of the gradient around a crease line (Fig. 3a), we want to filter the field in order to increase the degree of attraction/repulsion (Fig. 3b) and consequently its creaseness. At the same time, regions where there is neither a clear attraction nor

(a) (b)

Figure 3: Attraction and repulsion of vectors in (b) is higher than in (a).

repulsion must not change. This filtering can be carried out through the so–called *structure tensor*, which is a tool for analyzing oriented textures [4, 8].

Let's assume that at any given point $\mathbf{x}$ there is a single dominant orientation at most, taking into account a weighted neighborhood of size σ_{I} around it, $\mathcal{W}(\mathbf{x}; \sigma_{\mathrm{I}})$. The structure tensor is represented by the symmetric and semi-positive definite $d \times d$ matrix:

$$M(\mathbf{x}; \sigma_{\mathrm{I}}; \sigma_{\mathrm{D}}) = \mathcal{W}(\mathbf{x}; \sigma_{\mathrm{I}}) * (\mathbf{w}(\mathbf{x}; \sigma_{\mathrm{D}})^{\mathrm{t}} \mathbf{w}(\mathbf{x}; \sigma_{\mathrm{D}})) \tag{8}$$

where the convolution is element–wise. A suitable choice for the window is a d dimensional Gaussian, *i.e.* $\mathcal{W}(\mathbf{x}; \sigma_{\mathrm{I}}) = G(\mathbf{x}; \sigma_{\mathrm{I}})$. The dominant gradient orientation, namely $\mathbf{w}'$, is given by the eigenvector which corresponds to the highest eigenvalue of $\mathbf{M}$. However, in the structure tensor analysis, opposite directions are equally treated. Thus, to properly recover the direction in 2–d we put $\mathbf{w}'$ in the same quadrant that $\mathbf{w}$, and in 3–d in the same octant. Then, we obtain the new vector field:

$$\tilde{\mathbf{w}} = \mathrm{sign}(\mathbf{w}'^{\mathrm{t}} \mathbf{w}) \mathbf{w}' \tag{9}$$

where the function $\mathrm{sign}(x)$ returns $+1$ if $x > 0$, -1 if $x < 0$ and 0 if $x = 0$. In this way, attraction/repulsion of vectors is reinforced and the creaseness measure

$$\tilde{\kappa}_d = -\mathrm{div}(\tilde{\mathbf{w}}) \tag{10}$$

is enhanced along creases with respect to $\bar{\kappa}_d$. Again, $\tilde{\kappa}_d > 0$ means ridge and $\tilde{\kappa}_d < 0$ valley.

Table 1 shows the elapsed CPU times of the different operators for different image dimensions.

On the other hand, we have assumed that every point has a preferred orientation (the perpendicular to $\mathbf{w}'$). To check this assumption we associate to each orientation a confidence measure, normalized in the real interval $[0, 1]$ and such that it can be computed from the eigenvalues of the structure tensor. Similarity of eigenvalues implies isotropy, therefore $\mathcal{C}$ should be close to zero. For $\lambda_i, i = 1, ..., d$ being the eigenvalues of the structures tensor, a suitable confidence measure is:

$$\mathcal{C}(\mathbf{x}) = 1 - e^{-\left(\sum_{i=1}^{d} \sum_{j=i+1}^{d} (\lambda_i(\mathbf{x}) - \lambda_j(\mathbf{x}))^2 \right)^2 / 2c^2} \tag{11}$$

Table 1: CPU time in a 200 MHz Pentium Pro PC with 64MB of RAM, under Linux OS.

Image dimensions	Gaussian smoothing ($\sigma_D = 4.0$)	κ	$\bar{\kappa}$	$\mathcal{C}\tilde{\kappa}$
256^2	0.3 s	0.058 s	0.072 s	1.2 s
512^2	1.3 s	0.24 s	0.28 s	5.3 s
		κ_M	$\bar{\kappa}_M$	$\mathcal{C}\tilde{\kappa}_M$
$128^2 \times 84$	50 s	1.8 s	2.1 s	50 s
$250^2 \times 180$	360 s	23 s	23.3 s	720 s

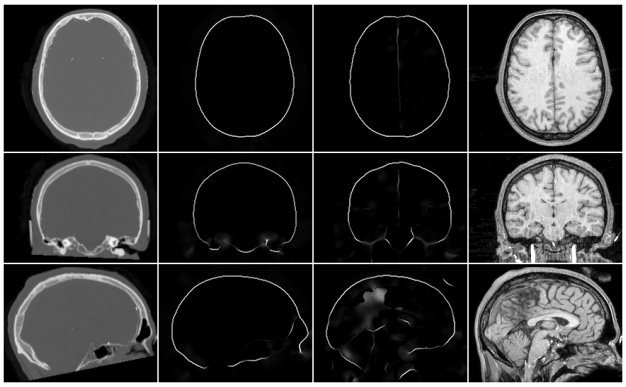

Figure 4: CT ridgeness and MR valleyness according to $\mathcal{C}\tilde{\kappa}_M$, for $\sigma_D = \sigma_I = 4.0$ voxels and $c = 1000$.

where threshold c is experimentally chosen. Then, $\mathcal{C}\tilde{\kappa}_d$ has a lower response that $\tilde{\kappa}_d$ at isotropic regions.

4 Automatic registration of CT and MR brain volumes

This application motivated our research on creaseness operators. We have focused on CT–MR registration because these modalities are widely available and provide partially complementary information (CT depicts accurately bones, while MR is suitable for soft tissues) which is interesting to fuse. Multisensor registration methods must take into account that images cannot be directly compared because the information they exhibit, though coming from a common origin, is not directly commensurable. First methods used markers visible in both modalities to provide good reference points, but they were manual and had the inconvenients of lacking retrospectiveness and not being patient friendly.

We have developed an automatic registration method similar to van den Elsen's [2]. It is based on the fact that the skull is visible both in CT and MR brain images. The signal produced by the bone

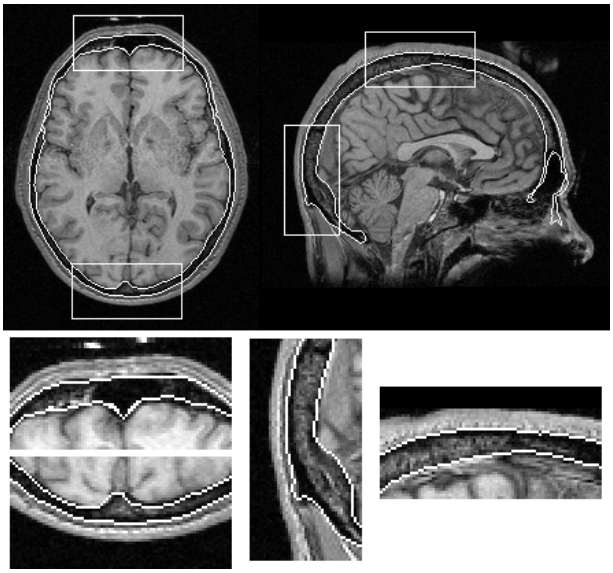

Figure 5: Contour of the skull from the registered CT overlapped to the MR volume. Here the contrast of the MR has been reduced to enhance the visibility of the contour.

is strong in CT, but weak in MR, in such a way that the skull forms a ridge surface in the CT image and a valley surface in the MR. Moreover, since the skull is an undeformable structure only rigid transformations need to be considered. Thus, only 6 parameters must be considered : θ_x, θ_y, θ_z for rotations around the correspondent axis and t_x, t_y, t_z for translations. Scaling factors are known from the acquisition system setting. Our work presents several improvements compared to the original van den Elsen's. Our creaseness operators $\bar{\kappa}_M$ and $\mathcal{C}\tilde{\kappa}_M$ yield a higher quality output. Currently we only use $\mathcal{C}\tilde{\kappa}_M$. Also, the transform parameters are optimized using the downhill simplex algorithm instead of exhaustive search. Finally, robustness has been assessed with a wider range and number of random transformations.

The first step of our registration procedure is to scale the CT and MR images to have voxels of the same size. Secondly we extract a ridgeness measure from the CT and a valleyness measure from the MR. The $\mathcal{C}\tilde{\kappa}_M$ operator is ideal for this purpose because it gives a very high and homogeneous response in the voxels depicting the center of the skull and avoids the discontinuities produced by other existing operators. This permits a quick convergence when aligning the images. The ridgeness from the CT image ($\mathcal{C}\tilde{\kappa}_M > 0$) and the valleyness from the MR ($\mathcal{C}\tilde{\kappa}_M < 0$) are extracted by using the same values of σ_D, σ_I and c (Fig. 4). The third step consists of iteratively trans-

Table 2: Parameter differences between T and T'. Angle differences are in degrees, translation and mean distance in millimeters. Results of our algorithm.

Δt_x	Δt_y	Δt_z	$\Delta\theta_x$	$\Delta\theta_y$	$\Delta\theta_z$	Mean dist.
0.00	0.00	0.00	0.00	0.00	0.00	0.00 +
0.09	0.01	0.07	0.03	0.06	0.15	0.25 –
0.03	0.02	0.19	0.11	0.02	0.05	0.22 +
0.05	0.04	0.15	0.07	0.03	0.05	0.17 +
0.10	0.02	0.25	0.13	0.02	0.04	0.29 –
0.11	0.02	0.29	0.10	0.04	0.08	0.32 –
1.77 *	0.50	0.51	0.06	0.13	0.93	2.36 – *
0.05	0.17	0.20	0.13	0.00	0.01	0.30 +
2.10 *	0.50	0.37	0.53	0.39	1.10	2.87 – *
0.01	0.13	0.15	0.08	0.07	0.00	0.24 +
0.10	0.27	0.18	0.12	0.00	0.01	0.40 +
0.18	0.06	0.21	0.10	0.04	0.01	0.34 –
0.16	0.11	0.28	0.06	0.12	0.00	0.39 –
0.07	0.06	0.19	0.10	0.06	0.01	0.23 +
0.11	0.15	0.19	0.07	0.11	0.09	0.33 +
0.09	0.05	0.26	0.03	0.10	0.03	0.30 –
0.32	0.45	0.04	0.06	0.05	0.11	0.63 +
0.13	0.14	0.15	0.12	0.02	0.08	0.31 –

Table 3: Parameter differences between T and T'. Angle differences are in degrees, translation and mean distance in millimeters. Results of the MI algorithm.

Δt_x	Δt_y	Δt_z	$\Delta\theta_x$	$\Delta\theta_y$	$\Delta\theta_z$	Mean dist.
0.51	0.05	0.51	0.05	0.15	0.00	0.86 –
0.01	0.12	0.09	0.00	0.01	0.01	0.16 +
0.12	0.18	0.04	0.04	0.06	0.02	0.26 –
0.25	0.33	0.14	0.05	0.01	0.00	0.43 –
0.20	0.01	0.01	0.04	0.04	0.06	0.28 +
0.02	0.19	0.08	0.08	0.06	0.06	0.28 +
0.07	0.23	0.00	0.01	0.04	0.04	0.27 +
0.04	0.39	0.16	0.15	0.10	0.19	0.56 –
0.01	0.06	0.08	0.08	0.02	0.29	0.46 +
0.18	0.32	0.04	0.06	0.17	0.19	0.50 –
0.17	0.40	0.05	0.21	0.21	0.36	0.72 –
0.07	0.07	0.01	0.04	0.02	0.03	0.14 +
0.09	0.30	0.03	0.04	0.03	0.08	0.36 +
0.02	0.21	0.02	0.04	0.01	0.05	0.25 –
0.20	0.03	0.15	0.05	0.16	0.24	0.43 –
0.03	0.03	0.03	0.06	0.01	0.03	0.09 +
0.40	0.25	0.08	0.02	0.04	0.29	0.68 –
0.02	0.06	0.02	0.01	0.01	0.02	0.08 +

form one of the images until it is properly aligned with the other. A proper function to measure the goodness of the alignment is the correlation $C_T = \sum_{\mathbf{x}\in f} f(\mathbf{x}) \cdot g(T(\mathbf{x}))$, where T represents a transformation whose parameters we want to test and f and g are the ridgeness and valleyness measure from the CT and MR images, respectively.

The function C_T together with the 6 parameters of the transformation defines a search space which is difficult to optimize because: a) the function is not monotonic, i.e. has many local maxima, b) the similarity measure is very expensive since it involves the transformation of a large image, and c) transformation parameters can not be decoupled. In order to search in lower dimensional spaces we can search the parameter space at multiple resolutions, as in [2]. The idea consists of searching for the best transformation at each level around the results found in the previous one. At the top of the pyramid, the search is done exhaustively to take advantage of its reduced dimensions. This search provides us with a set of candidate transforms. At the next level of the pyramid the algorithm starts a downhill simplex search [9] from each of the previous candidate transforms. This step generates new candidates that are supposed to be better than the previous ones. They are the seed for the downhill simplex in the next level of the pyramid. The process is repeated until the highest level of resolution is reached (bottom of the pyramid).

We devised an experiment to assess the robustness of the whole registration algorithm. We worked with a CT and MR scaled and unregistered pair of $250 \times 250 \times 180$ voxels. First we aligned both images to posteriorly unalign them through a transform T of known random parameters. We could recover the unknown alignment by a transform minimizing the mean square correspondence error of several stereotactic frame landmarks manually pointed out by experts [2]. However, the correspondence error of our transform is expected to have a similar magnitude to the one of the stereotactic frame approach. Thus, in order to objectively asses the accuracy of our method we registered the CT and MR images by running our algorithm. Let's denote as CT' and MR' these new registered images. Next, the CT' image was transformed using known parameters (transform T) and the registration algorithm was run in such a way that the MR' image was the one moved to perform the registration. Then, the algorithm recovers other parameters (transform T') that should be as closed as possible to the former ones. We ran this experiment using a number of different random transformations in order to ensure statistical significance. Transformation parameters took values randomly distributed within wide intervals, namely, ± 30 mm and $\pm 30°$ for each translation axis and rotation angles, respectively.

To asses the goodness of T' we measured the distance $\|T(\mathbf{x}) - T'(\mathbf{x})\|$ for each voxel $\mathbf{x}$ of the CT' image belonging to a region including the skull. Then we calculated the mean distance from all these voxels. This is quite reasonable because the skull is the structure of reference and far away from the center of

rotation. Table 2 shows the results of our algorithm for this experiment and Table 3 shows the results of the voxel–based method called mutual information (MI) [11], which currently is considered one of the best to register images from different modalities. In Table 2 the symbol '+' means that our algorithm performed better than MI and symbol '–' means worse. In Table 3, '+' means that MI performed better and '–' the opposite. The entries marked with '*' in Table 2 refer to the case where we did not obtained sub–pixel accuracy, which in both cases was due to a high error in recovering the translation along the x axis. We are currently addressing our efforts to discover the origin of this problem. Figure 5 displays a fusion result.

5 Conclusion

Level set extrinsic curvature is a creaseness measure that acts as medialness feature for grey–level objects. In this paper we have first pointed out the problem of discontinuities when computing it with the classical scheme. We have proposed an alternative that overcomes it. We have also proposed a modified version adapting the structure tensor filtering to improve the results. Finally, the operator has been used to register CT and MR brain volumes. The registration algorithm requires a hierarchic approach to deal with large volume images, as well as an optimization method (downhill simplex) to search for the best transformation. According to our experiments, we conclude that the resulting overall accuracy is in most cases sub–pixel and comparable to that achieved by the mutual information method. However, we still have to run more experiments with MR images of different contrast and CT images of fewer slices. Finally, since the creaseness measure $\mathcal{C}\tilde{\kappa}_{\mathrm{M}}$ looks like a thresholded image in the CT and the MR case, we want to transform it into a binary image and try also the surface–based registration approach.

Acknowledgments

This research has been partially funded by CICYT projects TIC97–1134–C02–02 and TAP96–0629–C04–03. The authors thank Dr. Petra van den Elsen from the 3D–CVG at the Utrecht University for providing two 3–d CT and MR datasets. We also thank Dr. Derek Hill and Dr. David Hawkers, from the Computational Imaging Science Group in Radiological Sciences, UMDS, Guy's and St. Thomas' Hospital, for allowing us the access to the mutual information registration software (written by Dr. Collin Studholme).

References

[1] D. Eberly, R. Gardner, B. Morse, S. Pizer, and C. Scharlach. Ridges for image analysis. *Journal of Mathematical Imaging and Vision*, 4:353–373, 1994.

[2] P. van den Elsen, A. Maintz, E-J. Pol, and M. Viergever. Automatic registration of CT and MR brain images using correlation of geometrical features. *IEEE Trans. on Medical Imaging*, 14:384–396, 1995.

[3] J. Gauch and S. Pizer. Multiresolution analysis of ridges and valleys in grey–scale images. *IEEE Trans. on Pattern Analysis and Machine Intelligence*, 15:635–646, 1993.

[4] B. Jahne. *Spatio–temporal image processing*, volume 751 of *Lecture Notes in Computer Science*, chapter 8, pages 143–152. Springer–Verlag, 1993.

[5] A. López and J. Serrat. Ridge/valley–like structures: creases, separatrices and drainage patterns. Technical Report 21, Computer Vision Center, campus of the Universitat Autònoma de Barcelona. Spain., 1997.

[6] A. Maintz. *Retrospective Registration of Tomographic Brain Images*. PhD thesis, Utrecht University, The Netherlands, 1996.

[7] O. Monga and S. Benayoun. Using partial derivatives of 3D images to extract typical surface features. *CVGIP: Image Understanding*, 61:171–189, 1995.

[8] W. Niessen, A. López, W. Van Enk, P. van Roermund, B. ter Haar Romeny, and M. Viergever. In vivo analysis of trabecular bone architecture. In J. Duncan and G. Gindi, editors, *Information Processing and Medical Imaging*, volume 1230 of *Lecture Notes in Computer Science*, pages 435–440, 1997.

[9] W. Press, S. Teukolsky, W. Vetterling, and B. Flannery. *Numerical Recipes in C*, chapter 10. Cambridge University Press, 1992.

[10] H. M. Schey. *DIV, GRAD, CURL and all that*, chapter 2. W. W. Norton and Company inc., 1973.

[11] D. Studholme, C. Hill and D. Hawkes. Automated 3D registration of MR and CT images of the head. *Medical Image Analysis*, 1:163–175, 1996.

[12] J. P. Thirion and A. Gourdon. Computing the differential characteristics of isointensity surfaces. *CVGIP: Image Understanding*, 61:190–202, 1995.